ES Energy & Environment

REVIEW PAPER View Article Online

Update on Recent Designing Strategies of Transition Metal-Based Layered Double Hydroxides Bifunctional Electrocatalysts

Zhengyang Cai, Ping Wang*, Junhe Yang and Xianying Wang*

Fabrication of efficient, stable and cost-effective bifunctional electrocatalysts to achieve overall water splitting reaction (OWS) has become a task of high priority, in view of the urgent need for the promotion of renewable energy-based hydrogen production systems. Transition metal-based layered double hydroxides (LDHs) as one of promising bifunctional electrocatalysts have been intensely studied, due to the advantages of unique 2D layered structure and outstanding physicochemical properties. Herein, this review aims to summarize the recently advanced strategies on design of LDHs, including nanostructuring, conductive support-based hybrid, defect engineering, anion intercalation, cation doping and related derivatives. Particularly, a thorough literature overview on OWS performance improvement of LDHs is appraised detailedly. The discussions on challenges and future directions are provided, which will shed light on development of better LDHs bifunctional electrocatalysts and exploration of efficient device units for practical applications.

Keywords: Layered Double Hydroxides; Bifunctional Electrocatalysts; Hydrogen Evolution Reaction; Oxygen Evolution Reaction; Overall Water Splitting

Received 20 May 2019**, Accepted** 20 July 2019

DOI: 10.30919/esee8c320

1. Introduction

Hydrogen production via water electrolysis is regarded as being a green and efficient technology.[1,2] However, the oxygen evolution reaction (OER) involving complex four-electron redox process is a challenging in water-splitting due to its sluggish kinetics.[3,4] It often requires electrocatalysts to reduce the overpotential and promote the reaction rate. Precious metal-based materials with the virtue of high activity are usually used as electrocatalysts for hydrogen evolution reaction (HER) (such as Pt or Pt/C) and oxygen evolution reaction (OER) (such as RuO_2 or IrO_2).[5-8] However, the disadvantages of high cost, scarcity, and poor stability greatly hinder the large scale implementation.[9,10] In the past few years, transition metal-based materials as electrocatalysts have been extensively studied, such as phosphides,[8,11-15] chalcogenides,[16-21] carbides,[22,23] and nitrides[24,25] for HER, and phosphates,[26,27] oxides,[28-33] hydroxides,[34-38] perovskite,[39] nitrides,[40-44] and chalcogenides[45-47] for OER. However, the ideal OWS system for commercial utilizations should be driven by one electrocatalytic material, which should be highly active and durable for both HER and OER in the same electrolyte solution. Thus, there is an urgent need to find highly efficient, stable and cost-effective bifunctional electrocatalysts that could lower the required overpotential for OWS and thereby reduce electric energy consumption.[48-50]

Among the developed electrocatalysts as outlined above, transition metal-based layered double hydroxides (LDHs) bifunctional electrocatalysts have gained a great deal of research attentions. As an important member of two-dimensional (2D) layered materials family, LDHs are typically composed of a positively charged hydrotalcite-like main layer and interlayer anions. The chemical formula can be expressed as $[M^{2+}_{1-x}M^{3+}_{x}(OH)_2][An^-]_{x/n}\cdot zH_2O$, where M^{2+} represents a divalent metal cation, M^{3+} represents a trivalent metal cation, and An^- are interlayer anions (Fig. 1b).[51-53] The unique 2D layered structure gives LDHs many advantages: i) metal cations can be flexibly tuned in the bulk layer; ii) types of interlayer anions can be exchangeable with controlled interlayer spaces; iii) by aid of external driving forces, like simple ultrasonication procedure, the increase of interlayer spaces and even the exfoliation of bulk LDHs into ultrathin nanosheets can be easily achieved.

The great achievements of LDHs in related electrocatalytic applications for HER or OER have been appraised in several excellent reviews.[52,54-57] The strategies on structural design and chemical modification of LDHs bifunctional electrocatalysts have been widely developed. However, to the best of our knowledge, the summary of LDHs as bifunctional electrocatalysts for OWS is rarely reported. This review will be mainly focused on the recent advances on designing strategies of LDHs bifunctional electrocatalysts for OWS. A brief summary on synthetic methods of LDHs bifunctional electrocatalysts and related electrocatalytic mechanism for OWS will be firstly given. Subsequently, the advanced design strategies of LDHs bifunctional electrocatalysts will be highlighted, including nanostructuring, conductive support-based hybrids, defect engineering, anion intercalation, cation doping and related LDHs derivatives. In the final section, the challenges and perspectives are proposed, which if fully addressed, will lead to substantial breakthroughs in optimized energy system configuration.

School of Materials Science and Technology, University of Shanghai for Science and Technology, Jungong Rd.516, 200093 Shanghai, China
***E-mail:** ping.wang@usst.edu.cn; xianyingwang@usst.edu.cn*

2. Basic electrocatalytic mechanism for alkaline overall water splitting

The OWS reaction (Eq. 3) contains two half-reactions, namely the cathodic HER (Eq. 4 and 5) and the anodic OER (Eq. 6 and 7), as shown in Fig. 1a. The catalytic mechanisms of HER and OER take place on the active sites (M) in alkaline media are also illustrated.

Ideally, an electrocatalytic reaction can occur when the applied voltage is equal to the equilibrium potential (E^0). However, due to the existence of reaction energy barriers, the electrocatalytic reaction can be carried out only when the applied potential (E) is higher than E^0. The overpotential (η) applied can be formulated as follow:

$$\eta = E - E^0 \quad (1)$$

And the relationship of current density (j) and applied overpotential (η) can be expressed by the Tafel equation as follow:

$$\eta = b \log(j/j_0) \quad (2)$$

where b is the Tafel slope, j_0 is the exchange current density which can be obtained when η = 0.

The Tafel slope not only indicates the growth rate of current density, but also can be used for inference of the rate-limiting step of electrocatalytic reactions.[55,58] Thus, the evaluation of an excellent bifunctional catalyst should be with a small η and a small b, which is desirable for both the HER and OER.

Moreover, the long-term stability of catalysts is also a very important index. Two kinds of measurement methods are usually applied to assess the stability of catalysts. The one is the chronopotentionmetry curves at constant current densities for a long period of time. The other one is to compare the LSV curves before and after a large amount of cyclic voltammetry cycles. In the harsh industrial applications the catalysts need to be stable for an extremely long time (tens of thousands of hours).[59, 60]

OWS:

$$2H_2O\ (l) \rightarrow 2H_2\ (g) + O_2\ (g) \quad (3)$$

HER (acidic solution):

$$2H^+\ (aq) + 2e^- \rightarrow H_2\ (g) \qquad (E^0 = 0\ V\ vs.\ RHE) \quad (4)$$

HER (neutral or alkaline solution):

$$2H_2O\ (l) + 2e^- \rightarrow H_2\ (g) + 2OH^-\ (aq) \qquad (E^0 = 0\ V\ vs.\ RHE) \quad (5)$$

OER (acidic solution):

$$2H_2O\ (l) \rightarrow 4H^+\ (aq) + O_2\ (g) + 4e^- \qquad (E^0 = 1.23\ V\ vs.\ RHE) \quad (6)$$

OER (neutral or alkaline solution):

$$4OH^-\ (aq) \rightarrow 2H_2O\ (l) + O_2\ (g) + 2e^- \qquad (E^0 = 1.23\ V\ vs.\ RHE) \quad (7)$$

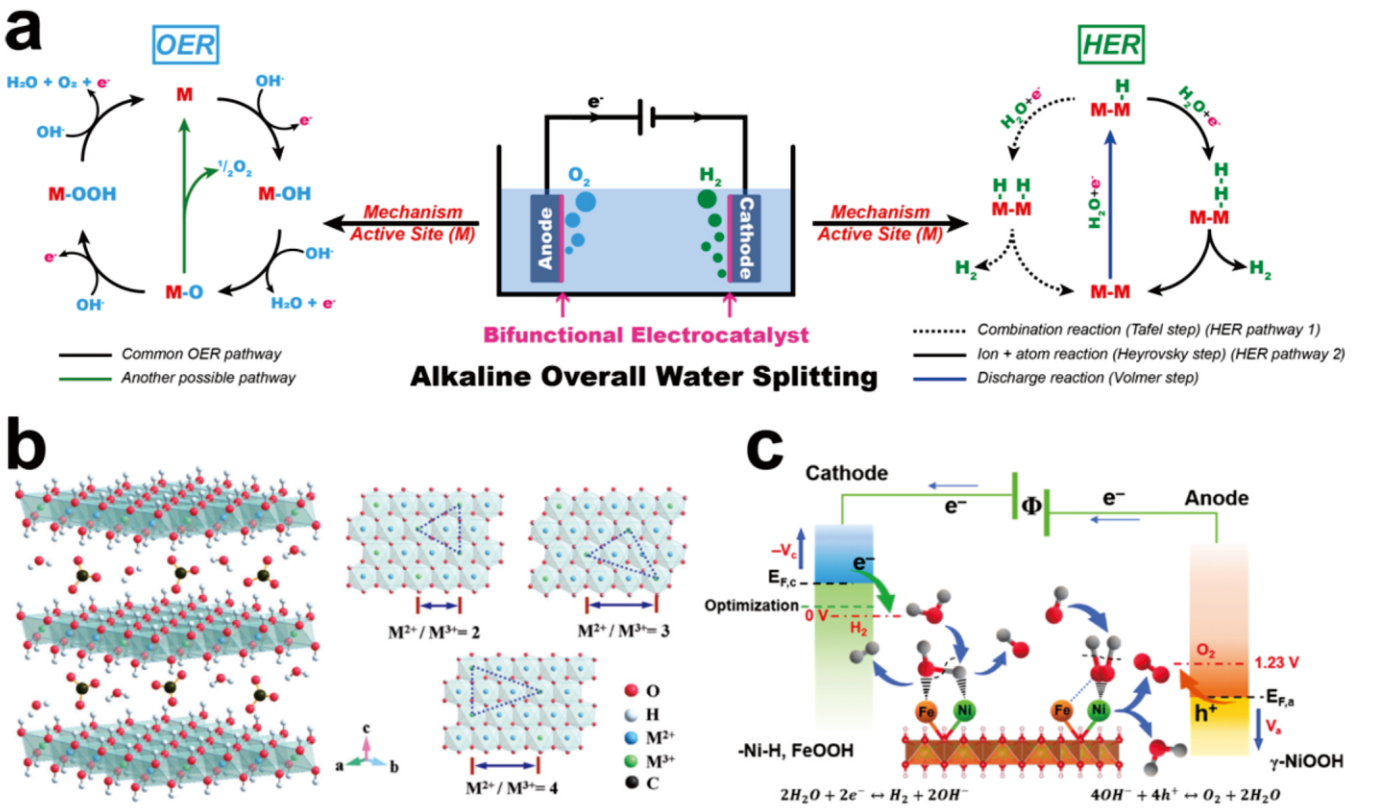

Fig. 1 a) Schematic illustration for alkaline overall water splitting reactions. b) The idealized structure of carbonate-intercalated LDHs with different M^{2+}/M^{3+} molar ratios showing the metal hydroxide octahedra stacked along the crystallographic c-axis, as well as water and anions present in the interlayer region. Reproduced with permission from Ref. 51. Copyright 2014, The Royal Society of Chemistry. c) Schematic representation of the electrocatalytic generation of H2 in alkaline media. FeOOH and Ni-H are the formed surface adsorbed intermediates during HER process, while, γ-NiOOH is the observed surface intermediate under OER process. Reproduced with permission from Ref. 61. Copyright 2019, The Royal Society of Chemistry.

To date, a large amount of research works have been put forward on studying the catalytic mechanism of LDHs, with development of cutting-edge characterization and simulation methods, such as operando X-ray absorption spectrum (XAS),[62,63] in-situ Raman,[61] in-situ transmission electron microscopy (TEM)[64] and density functional theory+U (DFT+U). Particularly for incorporation of heteroatoms in the LDH layers, the optimized doping ratio of different metal or non-metal elements in the LDH layer can greatly improve the intrinsic activity of the catalysts, that is, the electronic configuration of the metal sites (the exposed metal sites serve as active sites) can be adjusted, which can promote the synergistic effect among the active sites and thus improve the charge distribution in the LDH layer and the charge transfer capability. Furthermore, the correlation between Gibbs free energy of the reaction rate determining step and the enhancement in catalytic activity can be well established. For instance, the OWS mechanism of NiFe LDH via employment of in-situ Raman spectro-electrochemistry was proposed by Qiu *et al*.[61] The transformation of different active interfacial species during OER and HER unveiled the synergistic interaction between iron and nickel for facilitating water electrolysis processes (**Fig. 1c**).

3. Synthetic Approaches of LDHs Bifunctional Electrocatalysts

Several synthetic approaches have been explored for preparation of LDHs, mainly including coprecipitation, hydro/solvothermal synthesis, cathodic electrodeposition and electrospinning process (Table 1).[65] One of the most used methods is the coprecipitation method. Homogenous LDHs crystals can be quickly prepared by mixing metal salts mixture as precursors and aqueous alkaline solution at a constant temperature under sufficiently vigorous stirring.[66-68] Hydro/solvothermal synthetic methods are also usually employed by heating metal salts mixture and a weak alkali precipitant (such as urea,[69, 70] ammonia, methanol[71] or NaOH[72]) at a desired temperature in water/ organic solvents (such as ethanol[73] and dimethylformamide[74]). In the cases, the morphology and structure of LDHs can be easily controlled by pH value, reaction temperature and time. Moreover, cathodic electrodeposition method is more convenient and time-saving. Metal nitrate or sulfate can be used as electrolytes for providing a weak alkaline environment.[65, 75] However, it commonly suffers the difficulty in morphology control, leading to rough surfaces of the resulting LDHs.[76] The electrospinning technique, which is known to be simple, low-cost, and eco-friendly, is also adopted for preparation of LDHs with controllable nanofiber morphologies.[77]

4. Advanced Design Strategies for LDHs Bifunctional Electrocatalysts

It is well known that bulk thickness of LDHs with a large lateral size commonly suffered poor electrocatalytic performance, owing to the limited numbers of active sites with poor intrinsic activity and low electron conductivity.[78,79] In order to address these shortcomings, several design strategies have been developed (Table 2), specifically for nanostructuring, self-assembling on conductive substrates, defect engineering, ion-intercalation, cation doping and some related LDHs derivatives. In the chapter, the great successes gained with the respect to design strategies will be detailedly discussed.

4.1 Nanostructuring

Fabrication of hierarchical nanostructures or ultrathin nanosheets is of great benefit to maximize the number of active sites via increase of surface areas, and thus facilitate electrolyte diffusion and gases desorption.[79,115,116] Hu and co-workers meticulously designed a hierarchical Ni-Co-P hollow nanobrick (HNBs) comprised of oriented nanosheets (Fig. 2a and b).[83] By employing 3D Ag_2WO_4 anisotropic cuboids as sacrificial templates, HNBs were fabricated by growth of oriented 2D Ni-Co nanosheets precursor and subsequent etching/phosphorization treatments (Fig. 2c). The unique hierarchical and hollow structures were favorable for OWS performance enhancement of HNBs, as a result of significant increase in the exposed surface area and abundant mass diffusion pathways. Moreover, it was found that small amount of Ag residual also contributed to the increase in catalytic activity, based on the density functional theory (DFT) calculations (Fig. 2d and e). Upon incorporation of Ag, the ΔG_{H^*} became relatively close to 0 eV for the catalyst-H* state. It indicated that the faster proton/electron transfer/hydrogen release rate and the much larger water adsorption energy were realized, promoting HER processes.

Another interesting strategy is to fabricate self-standing 3D core-shell LDHs nanostructures. Cu nanowires@NiFe LDH nanosheets with a 3D core/shell structure were successfully synthesized via electrodeposition by Yu and the co-workers. for highly efficient OWS.[80] Cu nanowires (NWs) cores supported on Cu foams were firslty prepared by three-step pre-synthesis procedures, namely chemical oxidation, calcination for phase transformation and electroreduction processes. Subsequently, few-layer NiFe LDH nanosheets were grown on Cu NWs cores (Fig. 3a). As shown in Fig. 3b and c, the NiFe LDH uniformly and vertically grew on Cu NWs, forming a core-shell

Table 1 Common synthetic approaches for LDHs.

Approaches	Precursors	Temperature (^{o}C)	Morphology/ Structure	Cost
Coprecipitation	Metal salts, alkali solution	< 100	Bulk sheets, Crystal	Medium
Hydro/Solvothermal	Metal salts, precipitant, and solvent	80-120	Bulk sheets, Crystal	High
Electrodeposition	Metal salts and solvent	Room temperature	Few-layer nanosheets, Amorphous	Low
Electrospinning	Metal salts, conductive polymer and solvent	Room temperature	Nanofibers, Amorphous	Low

Table 2 Comparison of recently reported LDHs-based electrocatalysts for OWS in 1 M KOH aqueous solution.

Strategies	Electrocatalysts	Synthesis Method	Mass Loading ($mg \cdot cm^{-2}$)	η_{10}[c] (mV) OER / HER	Overall Voltage (V) @ 10 $mA \cdot cm^{-2}$	Tafel Slope ($mV \cdot dec^{-1}$) OER/HER	OWS Stability Time @ J $mA \cdot cm^{-2}$	Ref.	Year
Nanostructuring & Conductive support-based hybrids	Co@N-CS/N-HCP@CC	ECD[a] + Pseudomorphic Replic ation + Pyrolysis	3.20	248 / -66	1.545	68 / 65	24 h @ 30	80	2019
	Cu@NiFe LDH	Chemical oxidation + Calcination + Electroreduction + ECD	2.20	199 / -116	1.540	27.8 / 58.9	48 h @ 10	81	2017
	CoFe LDH-F	Delamination + Exfoliation	0.20	300 / -255	1.630	40 / 95	35 h @ 1.63 V	82	2016
	Ni–Co–P HNBs	Sacrificial template + Etching + Phosphorization	2.00	270 / -107	1.620	76 / 46	20 h @ 1.62 V	83	2018
	NiFe LDH@NiCoP/NF	HT[b] + Phosphorization + HT	2.00	220 / -120	1.570	88.2 / 48.6	100 h @ 10	84	2018
	Co_3S_4 @MoS_2	Sulfidation + Coating + Annealing	0.28	280 / -136	1.580	43 / 74	10 h @ 10	85	2018
	CoNi/$CoFe_2O_4$/NF	HT + Calcination + ECD	2.10	230 / -82	1.570	45 / 96	48 h @ 10	86	2018
	Cu@CoFe LDH	Chemical oxidation + Calcination + Electroreduction + EC D	1.80	240 / -171	1.681	44.4 / 36.4	48 h @ 10	87	2017
	$NiCo_2S_4$@NiFe LDH	HT + HT	——	201 @ η_{60} / -200	1.600	46.3 / 101.1	12 h @ 10	88	2017
	$NiCo_2O_4$ hollow microcuboids	Solvothermal + Annealing	1.00	230 @ η_1 / -50 @ η_1	1.650	53.0 / 49.7	36 h @ 10	89	2016
	VOOH nanospheres	HT	0.80	270 / -164	1.620	68 / 104	50 h @ 50	90	2017
	Ni_5Fe LDH@NF	HT	——	210 / -133	1.590	59 / 89	20 h @ 50	91	2017
	NiFe-LDH/$NiCo_2O_4$/NF	HT + Annealing + HT	4.90	290 @ η_{50} / -192	1.600	53 / 59	12 h @ 20	92	2017
	EG/$Co_{0.85}Se$/NiFe-LDH	Exfoliation + HT	4.00	270 @ η_{150} / -260	1.670	57 / 160	10 h @ 20	93	2015
	NiFe LDH-NS@DG10	Exfoliation + Stirring	2.00	210 / -115 @ η_{20}	1.5 @ 20 $mA \cdot cm^{-2}$	52 / 110	——	94	2017
	$NiCo_2P_x$/CNTs	Coprecipitation + Annealing	0.10	284 / -47	1.610	50.3 / 57.0	48 h @ 10	95	2018

	δ-FeOOH NSs/NF	Wet-chemical	0.16	265 / -108	1.620	36 / 68	60 h @ 1.73 V	96	2018
	$NiAl_8P$/NF	HT + Alkali -etching + Phosphorization	2.00	242 / -80	1.550	65 / 52	——	97	2018
Defect engineering	NiCoP/NF	HT + Plasma	1.60	280 / -32	1.580	87 / 37	24 h @ 10	98	2016
	Ni_3S_2@NiV-LDH/NF	HT + HT	0.71	190 / -126	1.530	57 / 90	160 h @ 10	99	2019
	N-NiCo LDHs/NCF	HT + Plasma	——	190 / -100	1.500	46 / 123	——	100	2019
	e-ICLDH@GDY/NF	HT + In-situ Exfoliation	——	216 / -43	1.430	43.6 / 98.9	60 h @ 1.56 V	101	2018
Intercalation	NiFe LDH-US	ECD + In -situ intercalation	——	203 / —	——	42 / —	——	102	2017
	$Na_{0.08}Ni_{0.9}Fe_{0.1}O_2$	Calcination + Chemical extraction	0.13	260 / —	——	40 / —	——	103	2016
	CoFe@NiFe-200/NF	HT + ECD	——	190 / -240	1.590	45.71 / 84.69	24 h @ 10	104	2019
Cation doping	NiFeIr LDH	HT	——	200 / -34	1.41 @ 20 $mA \cdot cm^{-2}$	— / 32	50 h @ 20	105	2018
	Mo-CoP	Wet-chemical + Phosphorization	2.50	305 / -40	1.560	56 / 65	20 h @ 1.5 V	106	2018
	PA-NiO	HT + Phosphorization	——	290 @ η_{60} / -138	1.560	36 / 81	7 h @ 1.6 V	107	2018
	FeCoNi-HNTAs	HT	1.00	184 / -58	1.429	49.9 / 37.5	100 h @ 1.59 V	108	2018
	Se-(NiCo)S/(OH)	HT	——	155 / -103	1.600	33.9 / 87.3	66 h @ 10	109	2018
	$NiCo_2S_4$	HT + HT	——	243 / -80	1.580	54.9 / 58.5	72 h @ 1.64 V	110	2019
LDHs Derivative	RuO_2/NiO/NF	HT + Impreganation + Calcination	1.10	250 / -22	1.500	50.5 / 31.7	25 h @ 10	111	2018
	FeCoP	ECD + Phosphorization	——	260 @ η_{20} / -188 @ η_{100}	1.600	63 / 76	20 h @ 1.606 V	112	2017
	MFN-MOFs/NF	Solvothermal	——	235 @ η_{50} / -79	1.495	55.4 / 30.1	100 h @ 500	113	2018
	Ni_2Cr_1-LDH/NF	HT	2	3 19 @ η_{100} / -67	1.550	22.9 / 61.5	30 h @ 1.55 V	114	2018

Note: [a] Electrochemical deposition, [b] Hydrothermal, [c] Overpotential required at the current density of 10 $mA \cdot cm^{-2}$.

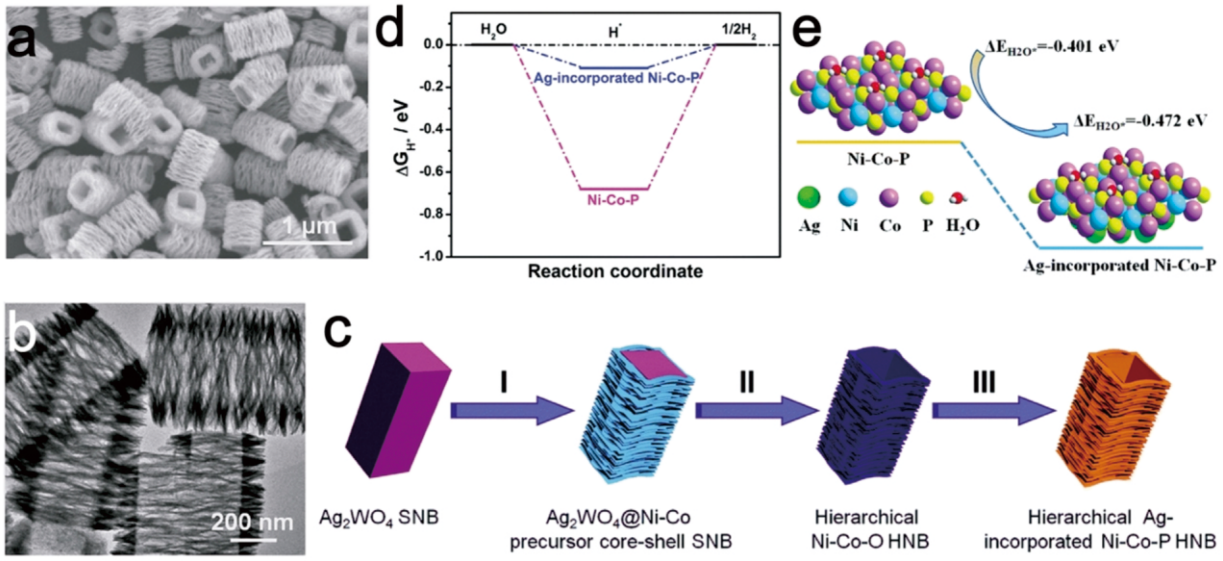

Fig. 2 a) FESEM and b) TEM images of Ni-Co-O HNBs, c) Schematic illustration of construction of hierarchical Ni-Co-P hollow nanobricks, d) Calculated free-energy change and e) water adsorption energies for Ni-Co-P and Ag-incorporated Ni-Co-P. Reproduced with permission from Ref. 83. Copyright 2018, The Royal Society of Chemistry.

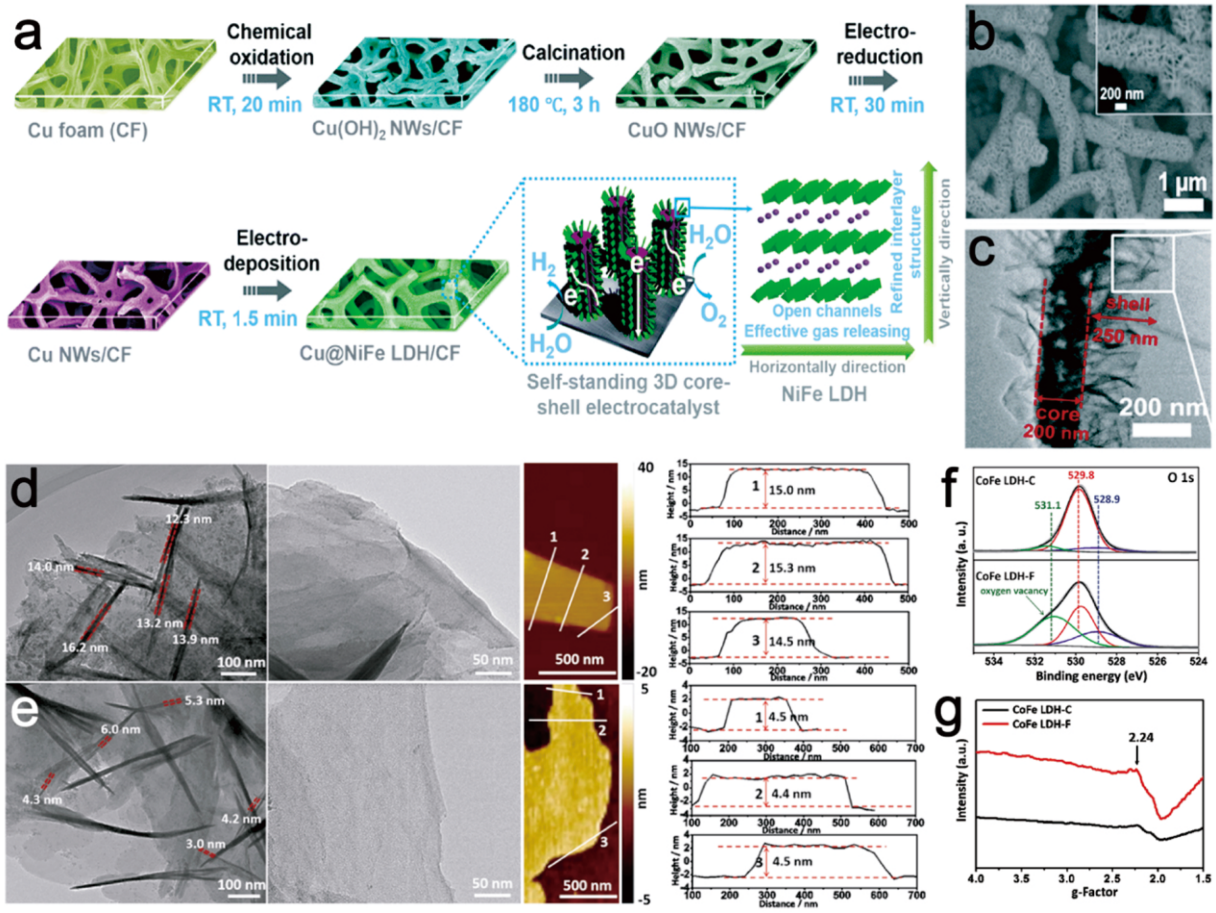

Fig. 3 a) Schematic illustration of the fabrication procedures of the self-standing 3D core-shell Cu@NiFe LDH electrocatalysts. (RT is denoted by room temperature.) b-c) SEM and TEM images of Cu@NiFe LDH. Reproduced with permission from Ref. 81. Copyright 2017, The Royal Society of Chemistry. d) TEM, AFM images and height profiles of CoFe LDH-C. e) TEM, AFM images and height profiles of CoFe LDH-F. f-g) O 1s XPS spectra and EPR spectra of the CoFe LDH-C and CoFe LDH-F samples, respectively. Reproduced with permission from Ref. 82. Copyright 2016, American Chemical Society.

structure. The Cu@NiFe LDH electrocatalyst exhibited excellent OWS performance, as listed in Table 2. It was attributed to the synergistic combination of NiFe LDHs and Cu NWs, which increased the edge sites exposure of LDHs and facilitated desorption of gases product, but also ensured good conductivity and mechanical stability.

Besides, an alternative approach to boost the OWS performance is to exfoliate bulk LDHs into ultrathin nanosheets. Liu and co-workers exfoliated CO_3^{2-} intercalated CoFe LDHs anions (CoFe LDH-C) in DMF-ethanol mixed solvents.[82] The resulted CoFe LDH-F possessed much smaller thickness of ~4.5 nm, compared to that of CoFe LDH-C (~15 nm) (Fig. 3d and e). During the exfoliation process, plentiful of coordination-unsaturated transition metals associated with oxygen vacancies were created, as demonstrated by X-ray photoelectron spectroscopy (XPS) and electron spin resonance (ESR) spectroscopy (Fig. 3f and g). The generated oxygen vacancies can decrease energy barrier for adsorption of OH^- anions, because of the low-coordination sites of MO_6 and improved intrinsic electronic conductivity, thus leading to small OER and HER overpotentials.

4.2 Conductive support-based hybrids

Self-supporting electrocatalysts on conductive substrates are an attractive approach for enhancing the number of catalytic active sites and the charge transfer ability, but also simplifying the electrode preparation process.[108,117-120] Hou *et al*. reported a ternary EG (exfoliated graphene foil)/$Co_{0.85}Se$/NiFe-LDH hybrid (Fig. 4a).[93] The field emission scanning electron microscopy (FESEM) images show the thickness of NiFe-LDHs grown on EG/$Co_{0.85}Se$ nanoarrays can be reduced to be about 10 nm (Fig. 4b-e). The catalyst with a high surface area of 156 $m^2 \cdot g^{-1}$ can achieve a current density of 20 $mA \cdot cm^{-2}$ at an external voltage of 1.71 V for OWS in a two-electrode cell (Table 2.). It was attributed to the strong coupling effect of the three components, ensuring low charge transfer resistance and fast vectorial electron-transport. Especially, the 3D layered structure could offer large amounts of active sites and accelerate gas bubbles release.

Taking the plentiful advantages of defective graphene (DG), like fast electron transfer kinetics, excellent stability and specific defect types, DG has been widely employed for OER and HER. Jia *et al*. reported the exfoliated NiFe LDHs nanosheets (NS)/DG by electrostatic stacking of positively charged NiFe LDH NS and negatively charged DG (Fig. 5a).[94] The different types of DG defects derived by the removal of heteroatoms from graphene acted as active sites, which can directly capture the transition metal atoms via strong π-π interaction and thus contribute to activities improvement for three basic electrochemical reactions (e.g., ORR, OER and HER). On the other hand, the charge distribution on the hybrid heterostructure was demonstrated by DFT calculation study (Fig. 5b and c). The electrons were re-distributed after assembling of NiFe LDH-NS and DG, and accumulated at the defect sites (blue dash frames in Fig. 5c). Therefore the outstanding OER and HER activities can be ascribed to the exfoliated NiFe LDH and the charge conductivity of DG.

Carbon nanotubes (CNTs) are also an effective substrate to enhance the electron transfer of LDHs. The electronegative oxygen functional groups on surface of CNTs can promote efficient dispersion of catalysts. Huang and co-workers constructed 3D nicke-cobalt bimetallic phosphide anchored on CNTs ($NiCo_2P_x$/CNTs). The catalyst exhibited enhanced catalytic performance toward both HER and OER (Fig. 5d).[95] The high electrocatalytic activity was attributed to the synergistic effect between $NiCo_2P_x$ and CNTs (Fig. 5e).

4.3 Defect engineering

In recent years, much attention has been paid to the defect engineering of LDHs,[72, 115, 121-124] i.e., creation of oxygen vacancies, cation vacancies and their mixture. Liu *et al*. in 2018 firstly proposed synthesis of ultrathin feroxyhyte nanosheets (δ-FeOOH NSs) with richful Fe vacancies (V_{Fe}).[96] The origin of the superior HER and OER reactivity of δ-FeOOH NSs was clearly validated. Introduction of V_{Fe} led to obvious upshift on the Fe K absorption edge of δ-FeOOH NSs (Fig. 6a), showing a reduction of the electron density of Fe atoms in NSs. As seen from the R space plot (Fig. 6b), first Fe-O shell was calculated to be a coordination number (N) of 5.5, which was close to the theoretical value of 6 for an octahedral and the second Fe-Fe shell in NSs was reduced by 20% to 1.6 in comparison with 2 for the bulk. It indicated the existence of rich V_{Fe} in δ-FeOOH NSs. It was also reflected by the upshift of Fe 2p peaks in δ-FeOOH NSs (Fig. 6c). The formation of V_{Fe} can activate the second neighboring surface Fe atom (Fe2 site). The

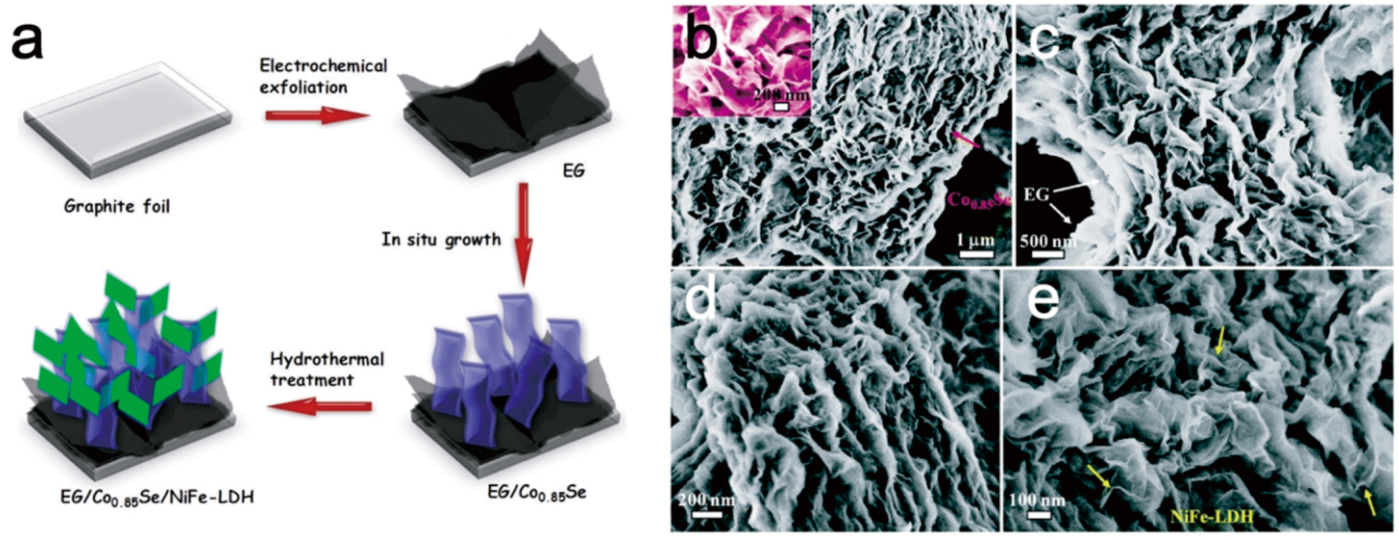

Fig. 4 a) Schematic illustration for the synthesis process of EG/$Co_{0.85}Se$/NiFe-LDH. b-c) FESEM images of EG/$Co_{0.85}Se$, Inset: the enlarged FESEM image of EG/$Co_{0.85}Se$. d-e) FESEM images of EG/$Co_{0.85}Se$/NiFe-LDH. Reproduced with permission from Ref. 93. Copyright 2016, The Royal Society of Chemistry.

DFT results also demonstrated that the Fe2 site had a small ΔG_{H^*}, giving rise to the enhanced HER performance of δ-FeOOH NSs (Fig. 6d). The Fe2 site acted as the OER active site, which possessed the smallest rate-determining ΔG value (Fig. 6e) and the four primitive OER steps on the electrocatalyst surface were proposed, as shown in Fig. 6f.

Cheng *et al*. developed a new type of 3D metal-vacancy-solid-solution NiAlP nanowall array ($NiAl_δP$) for all-pH OWS by combination of selective alkali-etching and phosphorization methods.[97] Numerous nanoholes were well distributed throughout each nanowall forming a unique porous structure and massive atomic vacancies are observed over the lattice of the NiAlP nanowalls (Fig. 7b and c). The XPS spectra revealed that the existence of surface aluminumvacancy led to a positive shift of 0.6 eV for Ni $2p_{3/2}$ and negative shift of 0.3 eV for P 2p (Fig. 7d and e). The theoretical calculations indicated that the $NiAl_δP$ possessed a low ΔG_{H^*} value -0.09 eV (close to that of Pt, ~0 eV) and the highest H_2O adsorption energy, favoring the water adsorption (Fig. 7f). The oxidized Ni and negatively charged P in $NiAl_δP$ might act as the active sites for OER and HER, respectively.

4.4 Ion intercalation

In addition to spontaneously inserting different anions or molecules into LDHs layers during preparation processes, the interlayer anions can be further replaced by using ion-exchange methods. It can enlarge the interlayer spacing, but also can exfoliate the bulk LDHs into monolayer or few-layer nanosheets which can increase the number of active sites and thus enhance catalytic activity.[125] Li *et al*. demonstrated an in-situ intercalation method to increase the interlayer spacing of NiFe LDHs (Fig. 8a).[102] As shown in Fig. 8b, XRD pattern shows that after formamide intercalation reaction at 80 °C for 3 h, the (003) diffraction peak of NiFe LDH shifted from 11.6° to t 9.3° (NiFe LDH-80 °C), corresponding to the increase of interlayer distance from 7.8 to 9.5 Å. With the assistance of ultrasound, the interlayer distance can increase to 9.3 Å at 30 ℃ for only 10 min (NiFe LDH-US-30 °C). The extended interlayer spacing offered more inner active sites and more space for diffusion of the reactants, the OER overpotential to achieve the current density of 10 $mA·cm^{-2}$ was reduced to 210 and 203 mV for NiFe LDH-80 °C and NiFe LDH-US-30 °C, compared to that of 256 mV for pristine NiFe LDH. Similarly, Na intercalated $NiFeO_x$ ($Na_{1-x}Ni_yFe_{1-y}O_2$) was also studied (Fig. 8c), consisting of $[MO_6]$ (M = Ni, Fe) octahedral layers with Na atoms residual lying between the octahedral layers.[103] The existence of Na led to transformation of Ni and Fe into high chemical states (Fig. 8d and e). Moreover, the extraction of Na gave

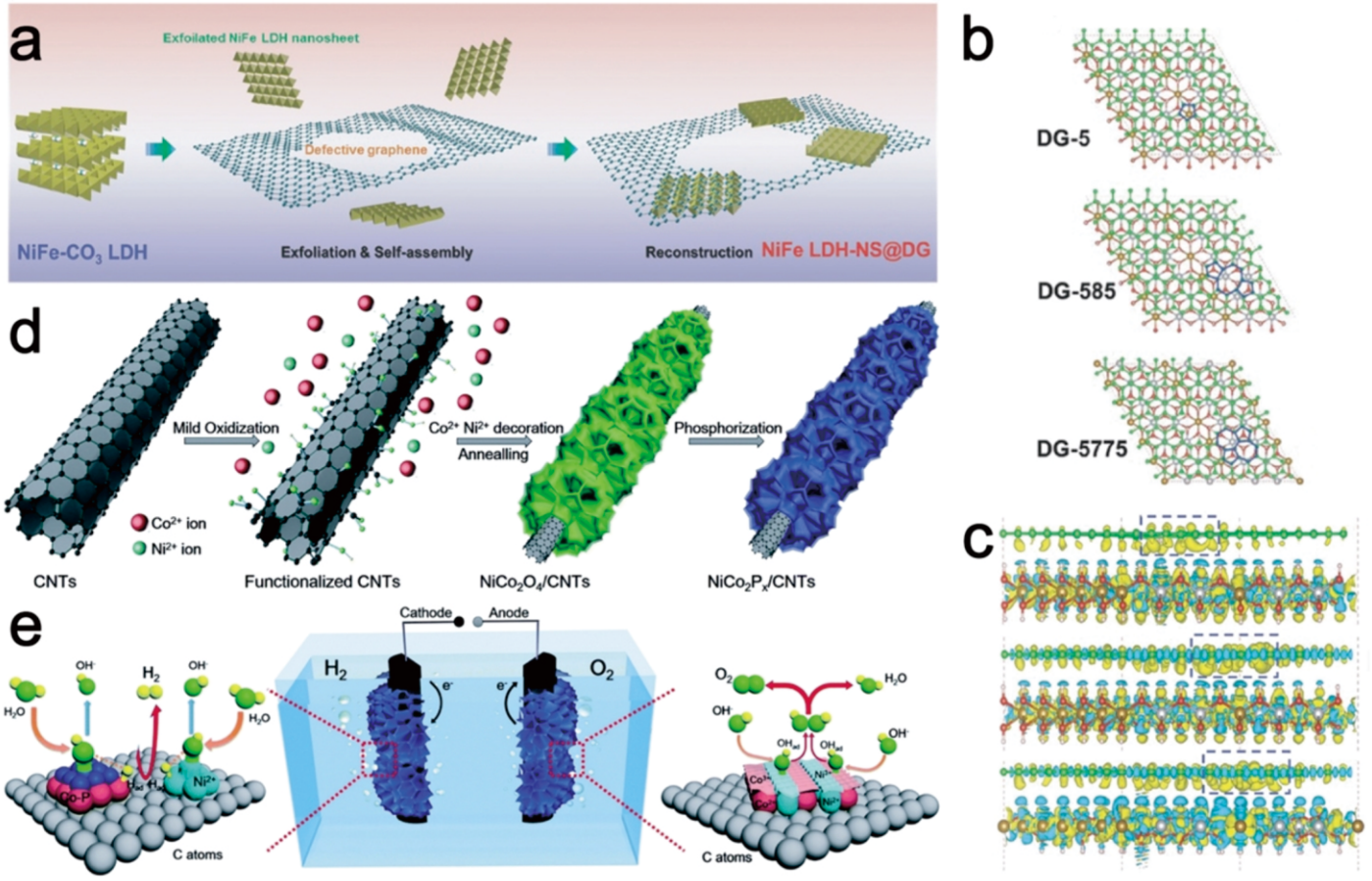

Fig. 5 a) Schematic illustration of the preparation of NiFe LDH-NS@DG nanocomposite. b) The top views of optimized Ni-Fe LDH-NS@DG (DG-5, DG-585, or DG-5775) based composite interfaces. c) The side views of 3D charge density difference plot for the interfaces between a defective graphene sheet (DG-5, DG-585 or DG-5775) and a Ni-Fe LDH-NS layer. Yellow and cyan isosurfaces represent the charge accumulation and depletion layers in the 3D space with an isosurface value of 0.002 e $Å^{-3}$. Green, brown, silver, and red balls represent C, Fe, Ni, and O atoms, respectively. The different defect types and associated enhanced charge density areas are marked with a blue solid line and a blue dash line, respectively. Reproduced with permission from Ref. 94. Copyright 2017, Wiley-VCH Verlag GmbH & Co. KGaA, Weinheim. d) Schematic illustration of the synthetic route for $NiCo_2P_x$/CNTs. e) Mechanism and the synergetic effect of $NiCo_2P_x$/CNTs for both the HER and OER. Reproduced with permission from Ref. 94. Copyright 2018, The Royal Society of Chemistry.

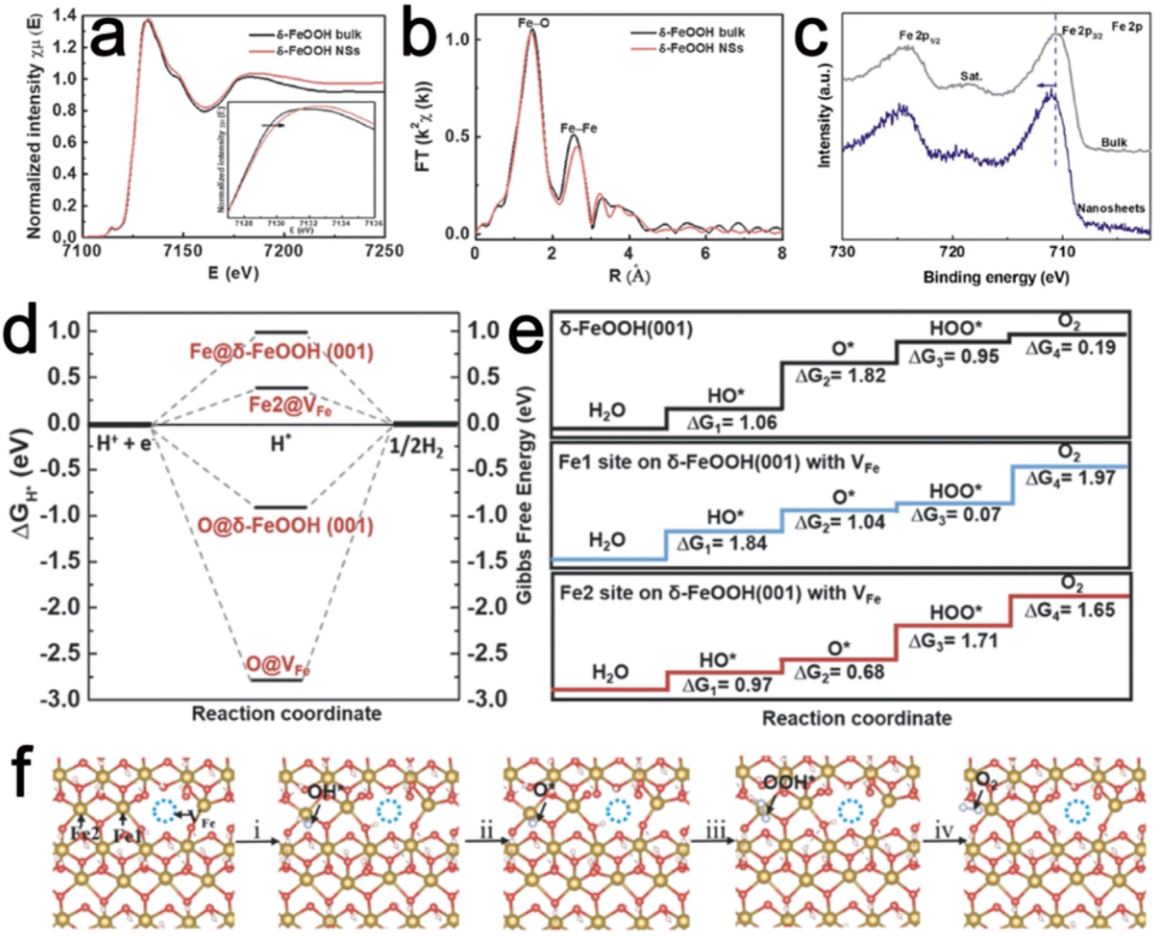

Fig. 6 a) Fe K-edge XANES spectra. b) the corresponding Fourier transformations of Fe K-edge EXAFS spectra for bulk δ-FeOOH and δ-FeOOH NSs. c) The high-resolution XPS spectra of Fe 2p of bulk δ-FeOOH and δ-FeOOH NSs. d) Standard free energy diagram of the HER process on the O and Fe in δ-FeOOH NSs without V_{Fe} (marked as δ-FeOOH (001)) and the O neighboring to V_{Fe} and the second neighboring Fe to V_{Fe} (Fe2) in δ-FeOOH NSs with V_{Fe} (marked as V_{Fe}). e) Standard free energy diagram of the OER processes on the δ-FeOOH (001), and Fe1 and Fe2 sites on δ-FeOOH (001) NSs with V_{Fe}. Fe1 indicates the first neighboring Fe to V_{Fe}, and Fe2 indicates the second neighboring Fe to V_{Fe}. f) Primitive steps of the OER process on the surface of δ-FeOOH NSs with V_{Fe} (top view). The Roman numerals represent (i) adsorption step, (ii and iii) dissociation steps, and (iv) desorption step during the OER process. Brown: Fe; red: O. Reproduced with permission from Ref. 96. Copyright 2018, Wiley-VCH Verlag GmbH & Co. KGaA, Weinheim.

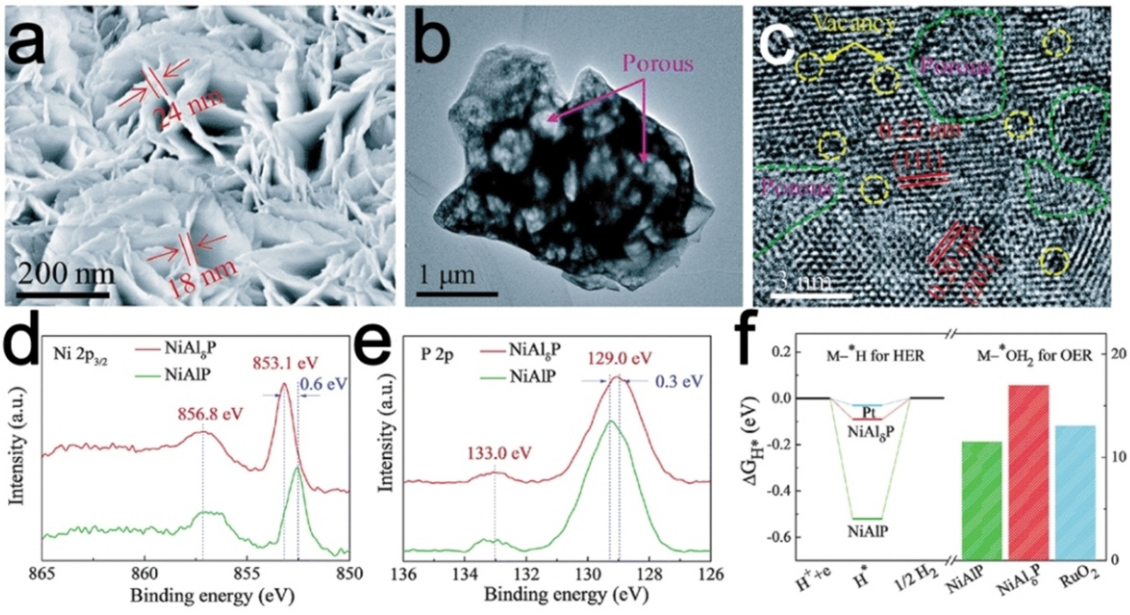

Fig. 7 a-c) SEM, TEN and HRTEM images for the $NiAl_\delta P$ nanowall array. d-e) Ni 2p and P 2p XPS spectra. f) Theoretical H* adsorption Gibbs free energy and H_2O* adsorption energy for NiAlP, $NiAl_\delta P$, and Pt or RuO_2. Reproduced with permission from Ref. 97. Copyright 2018, The Royal Society of Chemistry.

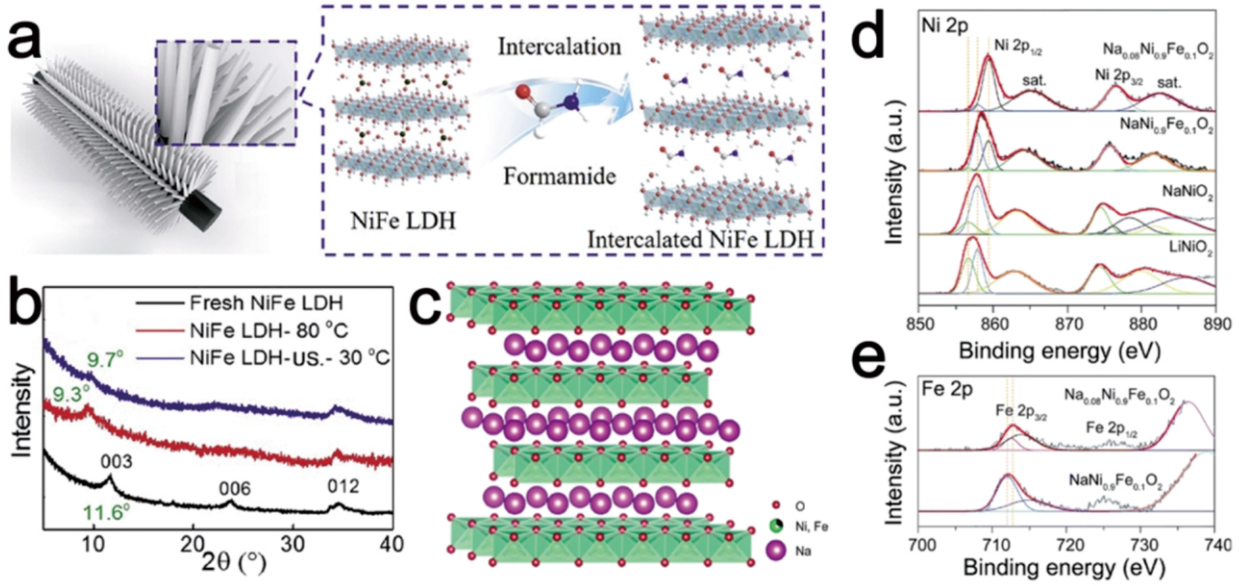

Fig. 8 a) Schematic diagram of in-situ intercalation process over electrodeposited NiFe LDH nanosheets on substrate. b) XRD patterns of the fresh NiFe LDH coated electrode (black) and intercalated NiFe LDH coated electrodes at 80 °C (red) and 30 °C with ultrasound (blue). Reproduced with permission from Ref. 102. Copyright 2017, Elsevier B.V. c) Crystal structure of O3-type $NaNi_yFe_{1-y}O_2$. d-e) Ni 2p and Fe 2p XPS spectra. Reproduced with permission from Ref. 103. Copyright 2017, The Royal Society of Chemistry.

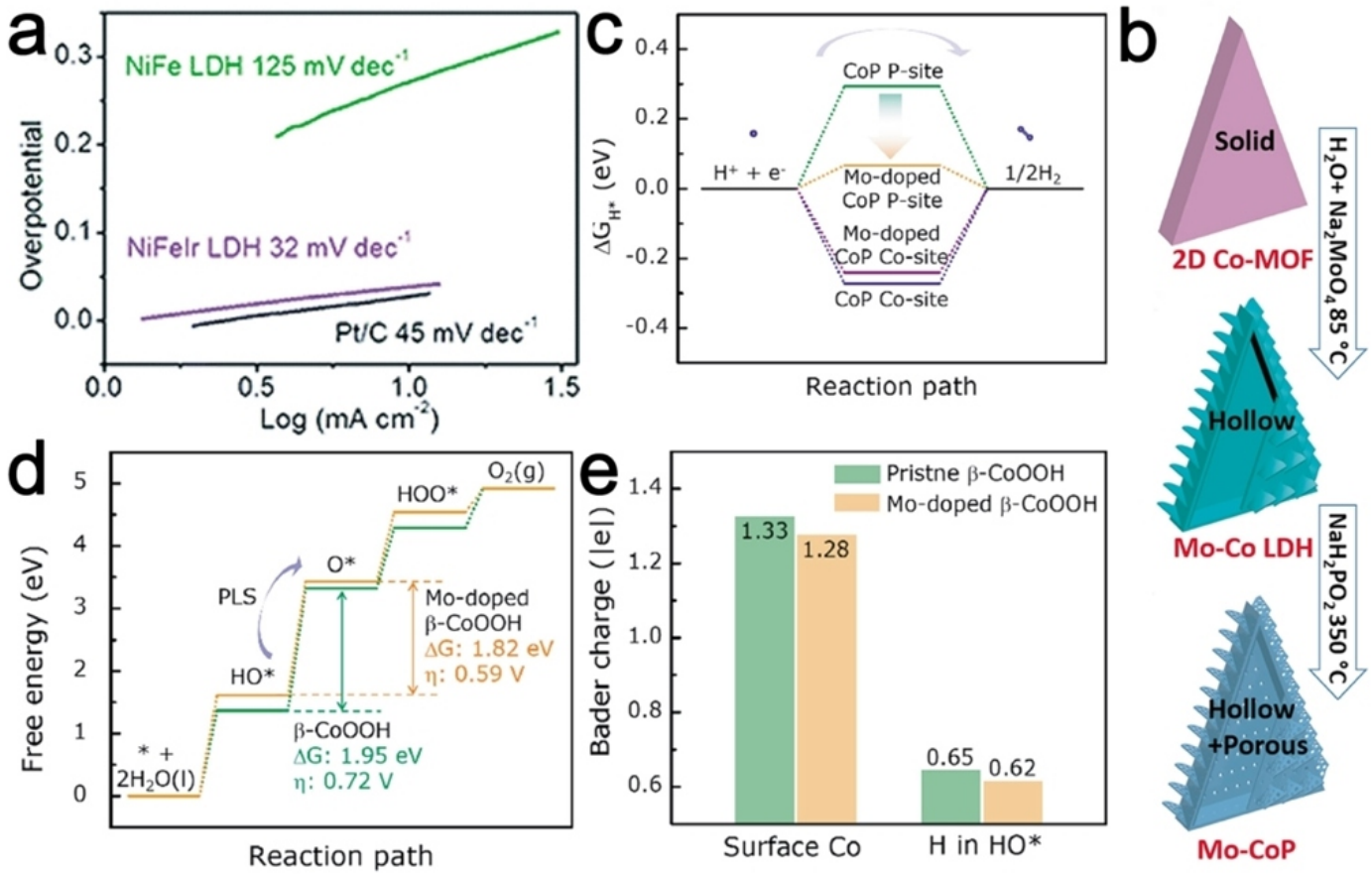

Fig. 9 a) Tafel slopes of NiFeIr LDH (violet), NiFe LDH (green) and Pt/C (black). Reproduced with permission from Ref. 105. Copyright 2018, The Royal Society of Chemistry. b) Schematic fabrication process and the resulting microstructures for hollow Mo-CoP nanoarrays. c) HER free energy diagrams for the P- and Co-sites on pristine and Mo-doped CoP (111) surfaces. d) Standard free energy diagrams for the OER path on pristine (green) and Mo-doped (orange) β-CoOOH (001) surfaces. e) Bader charge analysis for surface Co ions and H in HO*adsorption on pristine and Mo-doped β-CoOOH (001) surfaces. Reproduced with permission from Ref. 106. Copyright 2018, Elsevier B.V.

rise to the exposure of more [MO_6] active sites, leading to the improved activity. However, the excessive Na intercalation will deteriorate the structural stability.

4.5 Cation doping

Cation doping is considered to be an effective pathway for increasing OWS activity, since doping of the third metal ion can effectively adjust the electronic configuration and conductivity of LDHs and generate synergistic effect between metal ions and LDHs layers.[126-128] Chen and co-workers in 2018 reported a novel strategy to accelerate HER kinetics of NiFe LDH by Ir^{4+}-doping (NiFeIr LDHs). The water dissociation process (Volmer step) can be accelerated, thus leading to a robust catalytic activity for OWS.[105] The Tafel slope of NiFe LDH was estimated to be about 125 mV·dec^{-1} (Fig. 9a), indicating that the Volmer reaction ($H_2O + e^- \rightarrow H_{ad} + OH^-$) was the rate-determining step. While NiFeIr LDH possessed a much smaller Tafel slope of 32 m V·dec^{-1}, in accordance with the Volmer-Tafel mechanism ($H_2O + e^- \rightarrow H_{ad} + OH^-$, $2H_{ad} \rightarrow H_2$).

Rational design of hollow Mo-doped CoP (Mo-CoP) nanoarrays was recently proposed by Guan *et al*. (Fig. 9b).[106] DFT calculation results show the ΔG_{H^*} value of the P-site on Mo-CoP (111) surface dropped dramatically to 0.07 eV, indicating much superior HER performance (Fig. 9c). For OER (Fig. 9d) the potential limiting step (PLS) for β-CoOOH was determined to be the deprotonation step ($HO^* \rightarrow O^* + H^+ + e^-$). Accordingly, the ΔG_2 value was reduced from 1.95 eV to 1.82 eV by doping of Mo. As also evidenced by the reduced Bader charge of the Co and H (Fig. 9e), the electrons will transfer from Mo dopants to the nearby Co species and the H in HO* adsorption. The Mo-induced electron transfer towards the H can reduce the strength of the H-O bond in adsorbed HO*, thus facilitating the PLS process and enhancing the OER activity.

4.6 Other LDHs derivatives

Besides the above-mentioned design strategies, fabrication of LDHs

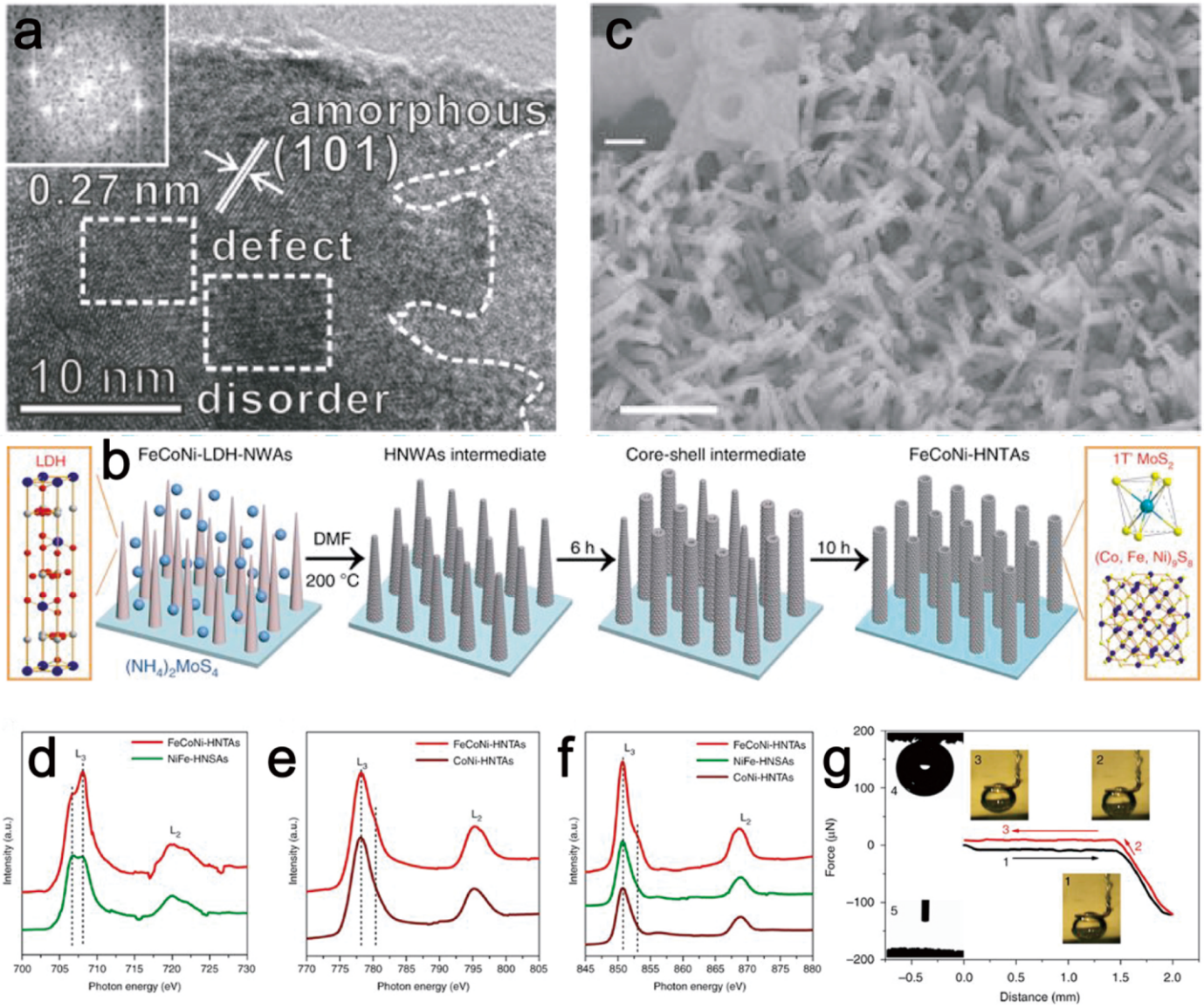

Fig. 10 a) HRTEM images of Se-(NiCo)S/OH nanosheets. Reproduced with permission from Ref. 109. Copyright 2018, Wiley-VCH Verlag GmbH & Co. KGaA, Weinheim. b) Schematic representation for synthetic procedure of FeCoNi-HNTAs. c) FESEM images of FeCoNi-HNTAs, Scale bars: 2 μm and inset: 200 nm. d-f) Normalized Fe, Co, and Ni L-edge sXAS spectra in the total electron yield (TEY) mode. g) Under-electrolyte Gas bubble adhesive force measurements of FeCoNi-HNTAs. Reproduced with permission from Ref. 108. Copyright 2018, Springer Nature Publishing AG.

derivatives is also of great interest by combination of two or multi design strategies for modification of LDHs (e.g. using multi-element doping and unique morphology design). Based on the theoretical expectations, transition metal chalcogenides (Se-(NiCo)S_x/$(OH)_x$ nanosheets) for highly efficient OWS was demonstrated by Hu *et al*.[109] A large amount of Se-O and S-O bonds can be formed in the nanosheets, which accelerated the charge transfer, and introduced abundant disordering and defects (Fig. 10a). Taking consideration of the remarkable electrocatalytic HER activity of metallic monoclinic 1T phase MoS_2 and excellent OER activity of trimetallic cobalt/iron/nickel-based (Co, Fe, Ni-based) sulfides, Li and co-workers reported synthesis of hybrid nanotube arrays (FeCoNi-HNTAs) composed of crystalline structures of 1T MoS_2 and (Co, Fe, Ni-based)$_9S_8$ (Fig. 10b and c).[108] The prominent activity was attributed to systematic optimization of chemical composition and geometric structure. Interestingly, the synergistic effects among Fe, Co and Ni ions were proved by aid of L-edge soft X-ray absorption spectroscopy (sXAS). Friebel *et al*.[127] further demonstrate that the Fe^{3+} indeed acted as the highly active sites for OER. The observation indicated that the Co ions can change the electronic state of Fe from Fe^{2+} to Fe^{3+} (Fig. 10d). The crystal-field coordination of Co ions can be tuned by Fe ions, that Co^{3+} ions located at octahedral sites (the small shoulder at 780.4 eV in FeCoNi-HNTAs) are the active centers for OER rather than the Co^{2+} ions at tetrahedral sites (778.2 eV) (Fig. 10e). And the XPS peak shoulder was also observed, indicating the existence of Ni^{3+} as the OER active sites (Fig. 10f). Furthermore, the FeCoNi-HNTAs electrodes showed prominent superaerophobicity and superhydrophilicity with no gases bubble adhesive force, which was greatly beneficial for gases evolution reaction and mass transfer (Fig. 10g).

4.7 Relevant applications

Although the electrocatalytic water electrolysis is regarded as a promising pathway for hydrogen production, the main obstacle remains the high energy consumption for potential practice. It is suggested that the effective, reliable and sustainable solution is to combine high-efficiency bifunctional OWS electrocatalysts with renewable energy sources, such as solar energy, wind energy, hydropower, etc. The renewable energy can be converted into hydrogen energy for storage, and then burn directly as fuel or used in more efficient fuel cell devices for electricity generation.

Many efforts have been devoted to exploiting the renewable energy-conversion systems, especially solar energy-based water splitting (Fig. 11).[94, 130-132] Luo and co-workers successfully designed an efficient and intrinsically safe bias-free solar-driven water-splitting device composed of perovskite light harvesters, non-precious metal based catalysts, and a bipolar membrane (Fig. 11a).[132] And a current density of 10 $mA \cdot cm^{-2}$ was obtained at the bias voltage of 1.63 V for electrochemical water splitting and the solar to hydrogen conversion efficiency is up to 12.7%. Other interesting case is to design hybrid LDHs via combined with semiconductor materials (like hematite,[131] $BiVO_4$,[133] g-C_3N_4,[135, 136] etc.) for photoelectrocatalytic water splitting. For instance, Yan's group successfully fabricated a triadic photoanode consisting of dual-sized CdTe quantum dots (QDs), Co-based layered double hydroxide (LDH) nanosheets and $BiVO_4$ particles (QD@LDH@$BiVO_4$). The catalyst possessed a remarkably enhanced PEC performance, achieving a current density of 2.23 $mA \cdot cm^{-2}$ at 1.23 V vs. RHE.[70]

5. Conclusions and outlook

Although the LDHs have been widely investigated for solely electrocatalytic HER or OER, poor electrocatalytic performance of bulk LDHs restrict the practical applications, owing to the limited numbers of active sites with poor intrinsic activity and low electron conductivity. Moreover, it remains challenging to the design criteria of LDHs bifunctional electrocatalysts for OWS. Therefore, this review summarizes the recent advanced design strategies of LDHs as bifunctional electrocatalysts for OWS. In the review, The current cutting-edge technologies for rational design of LDHs and related mechanisms are provided: (1) Fabrication of nanostructures can improve the density of active sites and enhance mass transfer capacity; (2) In-situ growth of LDHs on various conductive supports can enhance charge transport capacity; (3) Manufacture of various defects can regulate the surface electronic configuration of LDHs to increase the active site types and intrinsic activity; (4) Small molecules or ion

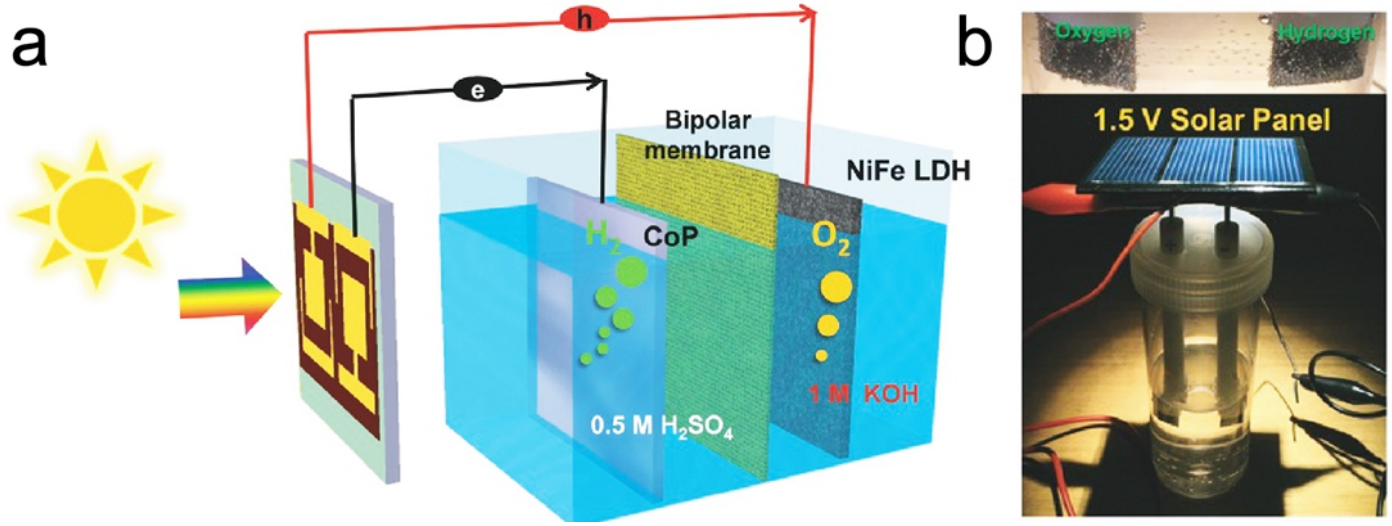

Fig. 11 a) Schematic diagram of the solar-driven water-splitting device composed of perovskite light harvesters, earth-abundant catalysts, and a bipolar membrane. Reproduced with permission from Ref. 132. Copyright 2016, Wiley-VCH Verlag GmbH & Co. KGaA, Weinheim. b) Demonstration of a solar power assisted water-splitting device with a voltage of 1.5 V. Reproduced with permission from Ref. 94. Copyright 2017, Wiley-VCH Verlag GmbH & Co. KGaA, Weinheim.

intercalation can expand the LDHs layer spacing to increase the number of active sites; (5) Cation doping can enhance the synergistic effect between different metal ions and thereby increase the intrinsic activity; (6) Development of related LDHs derivatives. These strategies not only improve the OER activity of LDHs, but also enhance their performance for HER, ultimately achieving the excellent OWS performance.

Despite these considerable efforts, there are still some challenges: (1) DFT methods are powerful in catalytic mechanism analysis of LDHs. However, it is hard to identify the actual active sites and determine the synergistic effect in more complexed catalyst components systems. Theoretical evaluation techniques still need to be continuously improved; (2) It is also expected that *in-situ* or operando characterization techniques, such as ambient-Pressure XPS, in situ XANES and in-situ Raman, can be fully applied to support the real-time mechanism analysis of catalytic reactions. Therefore, it should be considered to include highly efficient and well-structured electrolyzer systems; (3) Almost all LDHs bifunctional electrocatalysts can only run in alkaline environments. It is necessary to explore new strategies to make LDHs suitable for neutral or even acidic environments.

Conflicts of interest

There are no conflicts to declare.

Acknowledgements

We greatly appreciate the financial supports from the National Natural Science Foundation of China (51572173, 51602197, 51771121, 51772297 and 51702212), Shanghai Municipal Science and Technology Commission (16060502300, 16JC402200 and 18511110600), Shanghai Academic/Technology Research Leader Program (19XD1422900) and Shanghai Eastern Scholar Program (QD2016014).

References

1. S. Chu and A. Majumdar, *Nature*, 2012, **488**, 294-303.
2. G. Wu, A. Santandreu, W. Kellogg, S. Gupta, O. Ogoke, H. Zhang, H. L. Wang and L. Dai, *Nano Energy*, 2016, **29**, 83-110.
3. C. C. McCrory, S. Jung, I. M. Ferrer, S. M. Chatman, J. C. Peters and T. F. Jaramillo, *J. Am. Chem. Soc.*, 2015, **137**, 4347-4357.
4. J. Wang, W. Cui, Q. Liu, Z. Xing, A. M. Asiri and X. Sun, *Adv. Mater.*, 2016, **28**, 215-230.
5. T. Audichon, T. W. Napporn, C. Canaff, C. Morais, C. Comminges and K. B. Kokoh, *J. Phys. Chem. C*, 2016, **120**, 2562-2573.
6. M. Carmo, D. L. Fritz, J. Merge and D. Stolten, *Int. J. Hydrogen Energy*, 2013, **38**, 4901-4934.
7. S. Park, D. Yoon, S. Bang, J. Kim, H. Baik, H. Yang and K. Lee, *Nanoscale*, 2015, **7**, 15065-15069.
8. J. Tian, Q. Liu, A. M. Asiri and X. Sun, *J. Am. Chem. Soc.*, 2014, **136**, 7587-7590.
9. W. T. Hong, M. Risch, K. A. Stoerzinger, A. Grimaud, J. Suntivich and Y. Shao-Horn, *Energy Environ. Sci.*, 2015, **8**, 1404-1427.
10. T. Reier, Z. Pawolek, S. Cherevko, M. Bruns, T. Jones, D. Teschner, S. Selve, A. Bergmann, H. N. Nong, R. Schloegl, K. J. J. Mayrhofer and P. Strasser, *J. Am. Chem. Soc.*, 2015, **137**, 13031-13040.
11. D. Y. Chung, S. W. Jun, G. Yoon, H. Kim, J. M. Yoo, K. S. Lee, T. Kim, H. Shin, A. K. Sinha, S. G. Kwon, K. Kang, T. Hyeon and Y. E. Sung, *J. Am. Chem. Soc.*, 2017, **139**, 6669-6674.
12. P. Jiang, Q. Liu, Y. Liang, J. Tian, A. M. Asiri and X. Sun, *Angew. Chem. Int. Ed.*, 2014, **53**, 12855-12859.
13. J. Tian, Q. Liu, N. Cheng, A. M. Asiri and X. Sun, *Angew. Chem. Int. Ed.*, 2014, **53**, 9577-9581.
14. Z. Xing, Q. Liu, A. M. Asiri and X. Sun, *Adv. Mater.*, 2014, **26**, 5702-5707.
15. Z. H. Xue, H. Su, Q. Y. Yu, B. Zhang, H. H. Wang, X. H. Li and J. S. Chen, *Adv. Energy Mater.*, 2017, **7**, 1602355.
16. D. Kong, H. Wang, Z. Lu and Y. Cui, *J. Am. Chem. Soc.*, 2014, **136**, 4897-4900.
17. H. Li, C. Tsai, A. L. Koh, L. Cai, A. W. Contryman, A. H. Fragapane, J. Zhao, H. S. Han, H. C. Manoharan, F. Abild-Pedersen, J. K. Nørskov and X. Zheng, *Nat. Mater.*, 2015, **15**, 48.
18. C. Tang, N. Cheng, Z. Pu, W. Xing and X. Sun, *Angew. Chem. Int. Ed.*, 2015, **54**, 9351-9355.
19. D. Voiry, R. Fullon, J. Yang, C. de Carvalho Castro e Silva, R. Kappera, I. Bozkurt, D. Kaplan, M. J. Lagos, P. E. Batson, G. Gupta, Aditya D. Mohite, L. Dong, D. Er, V. B. Shenoy, T. Asefa and M. Chhowalla, *Nat. Mater.*, 2016, **15**, 1003.
20. A. Manikandan, P. R. Ilango, C. W. Chen, Y. C. Wang, Y. C. Shih, L. Lee, Z. M. Wang, H. Ko and Y. L. Chueh, *J. Mater. Chem. A*, 2018, **6**, 15320-15329.
21. A. Alarawi, V. Ramalingam, H. C. Fu, P. Varadhan, R. Yang and J. H. He, *Opt. Express*, 2019, **27**, A352-A363.
22. W. Cui, N. Cheng, Q. Liu, C. Ge, A. M. Asiri and X. Sun, *ACS Catal.*, 2014, **4**, 2658-2661.
23. A. Manikandan, L. Lee, Y. C. Wang, C. W. Chen, Y. Z. Chen, H. Medina, J. Y. Tseng, Z. M. Wang and Y. L. Chueh, *J. Mater. Chem. A*, 2017, **5**, 13320-13328.
24. B. Cao, G. M. Veith, J. C. Neuefeind, R. R. Adzic and P. G. Khalifah, *J. Am. Chem. Soc.*, 2013, **135**, 19186-19192.
25. Y. Wang, L. Chen, X. Yu, Y. Wang and G. Zheng, *Adv. Energy Mater.*, 2017, **7**, 1601390.
26. J. Xu, X. K. Wei, J. D. Costa, J. L. Lado, B. Owens-Baird, L. P. L. Gonçalves, S. P. S. Fernandes, M. Heggen, D. Y. Petrovykh, R. E. Dunin-Borkowski, K. Kovnir and Y. V. Kolen'ko, *ACS Catal.*, 2017, **7**, 5450-5455.
27. G. Zhang, G. Wang, Y. Liu, H. Liu, J. Qu and J. Li, *J. Am. Chem. Soc.*, 2016, **138**, 14686-14693.
28. G. S. Hutchings, Y. Zhang, J. Li, B. T. Yonemoto, X. Zhou, K. Zhu and F. Jiao, *J. Am. Chem. Soc.*, 2015, **137**, 4223-4229.
29. Y. Jin, H. Wang, J. Li, X. Yue, Y. Han, P. K. Shen and Y. Cui, *Adv. Mater.*, 2016, **28**, 3785-3790.
30. Q. Kang, L. Vernisse, R. C. Remsing, A. C. Thenuwara, S. L. Shumlas, I. G. McKendry, M. L. Klein, E. Borguet, M. J. Zdilla and D. R. Strongin, *J. Am. Chem. Soc.*, 2017, **139**, 1863-1870.
31. Y. Lee, J. Suntivich, K. J. May, E. E. Perry and Y. Shao-Horn, *J. Phys. Chem. Lett.*, 2012, **3**, 399-404.
32. F. Lyu, Y. Bai, Z. Li, W. Xu, Q. Wang, J. Mao, L. Wang, X. Zhang and Y. Yin, *Adv. Funct. Mater.*, 2017, **27**, 1702324.
33. G. Wu, W. Chen, X. Zheng, D. He, Y. Luo, X. Wang, J. Yang, Y. Wu, W. Yan, Z. Zhuang, X. Hong and Y. Li, *Nano Energy*, 2017, **38**, 167-174.
34. M. Gao, W. Sheng, Z. Zhuang, Q. Fang, S. Gu, J. Jiang and Y. Yan, *J. Am. Chem. Soc.*, 2014, **136**, 7077-7084.
35. W. Liu, H. Liu, L. Dang, H. Zhang, X. Wu, B. Yang, Z. Li, X. Zhang, L. Lei and S. Jin, *Adv. Funct. Mater.*, 2017, **27**, 1603904.
36. X. Long, J. Li, S. Xiao, K. Yan, Z. Wang, H. Chen and S. Yang, *Angew. Chem. Int. Ed.*, 2014, **53**, 7584-7588.
37. M. Tahir, N. Mahmood, L. Pan, Z. F. Huang, Z. Lv, J. Zhang, F. K. Butt, G. Shen, X. Zhang, S. X. Dou and J. J. Zou, *J. Mater. Chem. A*, 2016, **4**, 12940-12946.
38. Y. Li, L. Zhang, X. Xiang, D. Yan and F. Li, *J. Mater. Chem. A*, 2014, **2**, 13250-13258.
39. J. I. Jung, H. Y. Jeong, J. S. Lee, M. G. Kim and J. Cho, *Angew. Chem. Int. Ed.*, 2014, **53**, 4582-4586.
40. Y. Fan, S. Ida, A. Staykov, T. Akbay, H. Hagiwara, J. Matsuda, K. Kaneko and T. Ishihara, *Small*, 2017, **13**, 1700099.
41. K. Xu, P. Chen, X. Li, Y. Tong, H. Ding, X. Wu, W. Chu, Z. Peng, C. Wu and Y. Xie, *J. Am. Chem. Soc.*, 2015, **137**, 4119-4125.
42. F. Yu, H. Zhou, Z. Zhu, J. Sun, R. He, J. Bao, S. Chen and Z. Ren, *ACS Catal.*, 2017, **7**, 2052-2057.
43. Y. Zhang, B. Ouyang, J. Xu, G. Jia, S. Chen, R. S. Rawat and H. J. Fan, *Angew. Chem. Int. Ed.*, 2016, **55**, 8670-8674.
44. X. Zhao, F. Li, R. Wang, J. M. Seo, H. J. Choi, S. M. Jung, J. Mahmood, I. Y. Jeon and J. B. Baek, *Adv. Funct. Mater.*, 2017, **27**, 1605717.
45. Y. Liu, H. Cheng, M. Lyu, S. Fan, Q. Liu, W. Zhang, Y. Zhi, C. Wang, C. Xiao, S. Wei, B. Ye and Y. Xie, *J. Am. Chem. Soc.*, 2014, **136**, 15670-15675.
46. T. Yoon and K. S. Kim, *Adv. Funct. Mater.*, 2016, **26**, 7386-7393.
47. J. Wan, W. Ye, R. Gao, X. Fang, Z. Guo, Y. Lu and D. Yan, *Inorg. Chem.*

Front., 2019, **6**, 1793-1798.
48. X. Fan, Y. Liu, S. Chen, J. Shi, J. Wang, A. Fan, W. Zan, S. Li, W. A. Goddard and X. M. Zhang, *Nat. Commun.*, 2018, **9**, 1809.
49. P. W. Menezes, C. Panda, S. Loos, F. Bunschei-Bruns, C. Walter, M. Schwarze, X. Deng, H. Dau and M. Driess, *Energy Environ. Sci.*, 2018, **11**, 1287-1298.
50. F. Yu, H. Zhou, Y. Huang, J. Sun, F. Qin, J. Bao, W. A. Goddard, S. Chen and Z. Ren, *Nat. Commun.*, 2018, **9**, 2551.
51. G. Fan, F. Li, D. G. Evans and X. Duan, *Chem. Soc. Rev.*, 2014, **43**, 7040-7066.
52. Q. Wang and D. O'Hare, *Chem. Rev.*, 2012, **112**, 4124-4155.
53. S. M. Xu, T. Pan, Y. B. Dou, H. Yan, S. T. Zhang, F. Y. Ning, W. Y. Shi and M. Wei, *J. Phys. Chem. C*, 2015, **119**, 18823-18834.
54. A. Sengeni, K. K and S. Kundu, *Mater. Today Energy*, 2017, **6**, 1-26.
55. Y. Wang, D. Yan, S. El Hankari, Y. Zou and S. Wang, *Adv. Sci.*, 2018, **5**, 1800064.
56. R. Gao and D. Yan, *Adv. Energy Mater.*, 2019, **0**, 1900954.
57. A. Alarawi, V. Ramalingam and J. H. He, *Mater. Today Energy*, 2019, **11**, 1-23.
58. Y. Li, H. Wang, L. Xie, Y. Liang, G. Hong and H. Dai, *J. Am. Chem. Soc.*, 2011, **133**, 7296-7299.
59. I. Dincer and C. Acar, *Int. J. Hydrogen Energy*, 2015, **40**, 11094-11111.
60. A. Li, H. Ooka, N. Bonnet, T. Hayashi, Y. Sun, Q. Jiang, C. Li, H. Han and R. Nakamura, *Angew. Chem.*, 2019, **131**, 5108-5112.
61. Z. Qiu, C. W. Tai, G. A. Niklasson and T. Edvinsson, *Energy Environ. Sci.*, 2019, **12**, 572-581.
62. Z. Cai, D. Zhou, M. Wang, S. M. Bak, Y. Wu, Z. Wu, Y. Tian, X. Xiong, Y. Li, W. Liu, S. Siahrostami, Y. Kuang, X. Q. Yang, H. Duan, Z. Feng, H. Wang and X. Sun, *Angew. Chem.*, 2018, **130**, 9536-9540.
63. C. Wei, Z. Feng, M. Baisariyev, L. Yu, L. Zeng, T. Wu, H. Zhao, Y. Huang, M. J. Bedzyk, T. Sritharan and Z. J. Xu, *Chem. Mater.*, 2016, **28**, 4129-4133.
64. J. Yang, Z. Zeng, J. Kang, S. Betzler, C. Czarnik, X. Zhang, C. Ophus, C. Yu, K. Bustillo, M. Pan, J. Qiu, L. W. Wang and H. Zheng, *Nat. Mater.*, 2019, DOI: 10.1038/s41563-019-0415-3.
65. F. Dionigi and P. Strasser, *Adv. Energy Mater.*, 2016, **6**, 1600621.
66. O. Diaz-Morales, I. Ledezma-Yanez, M. T. M. Koper and F. Calle-Vallejo, *ACS Catal.*, 2015, **5**, 5380-5387.
67. M. A. Oliver-Tolentino, J. Vázquez-Samperio, A. Manzo-Robledo, R. D. G. González-Huerta, J. L. Flores-Moreno, D. Ramírez-Rosales and A. Guzmán-Vargas, *J. Phys. Chem. C*, 2014, **118**, 22432-22438.
68. R. Gao and D. Yan, *Nano Research*, 2018, **11**, 1883-1894.
69. Z. Lu, W. Xu, W. Zhu, Q. Yang, X. Lei, J. Liu, Y. Li, X. Sun and X. Duan, *Chem. Commun.*, 2014, **50**, 6479-6482.
70. Y. Tang, R. Wang, Y. Yang, D. Yan and X. Xiang, *ACS Appl. Mater. Interfaces*, 2016, **8**, 19446-19455.
71. H. Chen, L. Hu, M. Chen, Y. Yan and L. Wu, *Adv. Funct. Mater.*, 2014, **24**, 934-942.
72. R. Liu, Y. Wang, D. Liu, Y. Zou and S. Wang, *Adv. Mater.*, 2017, **29**, 1701546.
73. W. Yang, Z. Gao, J. Wang, J. Ma, M. Zhang and L. Liu, *ACS Appl. Mater. Interfaces*, 2013, **5**, 5443-5454.
74. M. Gong, Y. Li, H. Wang, Y. Liang, J. Z. Wu, J. Zhou, J. Wang, T. Regier, F. Wei and H. Dai, *J. Am. Chem. Soc.*, 2013, **135**, 8452-8455.
75. Y. Tang, X. Fang, X. Zhang, G. Fernandes, Y. Yan, D. Yan, X. Xiang and J. He, *ACS Appl. Mater. Interfaces*, 2017, **9**, 36762-36771.
76. Z. Cai, X. Bu, P. Wang, J. C. Ho, J. Yang and X. Wang, *J. Mater. Chem. A*, 2019, **7**, 5069-5089.
77. Z. Guo, W. Ye, X. Fang, J. Wan, Y. Ye, Y. Dong, D. Cao and D. Yan, *Inorg. Chem. Front.*, 2019, **6**, 687-693.
78. J. Ji, L. L. Zhang, H. Ji, Y. Li, X. Zhao, X. Bai, X. Fan, F. Zhang and R. S. Ruoff, *ACS Nano*, 2013, **7**, 6237-6243.
79. F. Song and X. Hu, *Nat. Commun.*, 2014, **5**, 4477.
80. Z. Chen, Y. Ha, H. Jia, X. Yan, M. Chen, M. Liu and R. Wu, *Adv. Energy Mater.*, 2019, **0**, 1803918.
81. L. Yu, H. Zhou, J. Sun, F. Qin, F. Yu, J. Bao, Y. Yu, S. Chen and Z. Ren, *Energy Environ. Sci.*, 2017, **10**, 1820-1827.
82. P. F. Liu, S. Yang, B. Zhang and H. G. Yang, *ACS Appl. Mater. Interfaces*, 2016, **8**, 34474-34481.
83. E. Hu, Y. Feng, J. Nai, D. Zhao, Y. Hu and X. W. Lou, *Energy Environ. Sci.*, 2018, **11**, 872-880.
84. H. Zhang, X. Li, A. Hähnel, V. Naumann, C. Lin, S. Azimi, S. L. Schweizer, A. W. Maijenburg and R. B. Wehrspohn, *Adv. Funct. Mater.*, 2018, **28**, 1706847.
85. Y. Guo, J. Tang, Z. Wang, Y. M. Kang, Y. Bando and Y. Yamauchi, *Nano Energy*, 2018, **47**, 494-502.
86. S. Li, S. Sirisomboonchai, A. Yoshida, X. An, X. Hao, A. Abudula and G. Guan, *J. Mater. Chem. A*, 2018, **6**, 19221-19230.
87. L. Yu, H. Zhou, J. Sun, F. Qin, D. Luo, L. Xie, F. Yu, J. Bao, Y. Li, Y. Yu, S. Chen and Z. Ren, *Nano Energy*, 2017, **41**, 327-336.
88. J. Liu, J. Wang, B. Zhang, Y. Ruan, L. Lv, X. Ji, K. Xu, L. Miao and J. Jiang, *ACS Appl. Mater. Interfaces*, 2017, **9**, 15364-15372.
89. X. Gao, H. Zhang, Q. Li, X. Yu, Z. Hong, X. Zhang, C. Liang and Z. Lin, *Angew. Chem. Int. Ed.*, 2016, **55**, 6290-6294.
90. H. Shi, H. Liang, F. Ming and Z. Wang, *Angew. Chem. Int. Ed.*, 2017, **56**, 573-577.
91. Y. Zhang, Q. Shao, Y. Pi, J. Guo and X. Huang, *Small*, 2017, **13**, 1700355.
92. Z. Wang, S. Zeng, W. Liu, X. Wang, Q. Li, Z. Zhao and F. Geng, *ACS Appl. Mater. Interfaces*, 2017, **9**, 1488-1495.
93. Y. Hou, M. R. Lohe, J. Zhang, S. Liu, X. Zhuang and X. Feng, *Energy Environ. Sci.*, 2016, **9**, 478-483.
94. Y. Jia, L. Zhang, G. Gao, H. Chen, B. Wang, J. Zhou, M. T. Soo, M. Hong, X. Yan, G. Qian, J. Zou, A. Du and X. Yao, *Adv. Mater.*, 2017, **29**, 1700017.
95. C. Huang, T. Ouyang, Y. Zou, N. Li and Z. Q. Liu, *J. Mater. Chem. A*, 2018, **6**, 7420-7427.
96. B. Liu, Y. Wang, H. Q. Peng, R. Yang, Z. Jiang, X. Zhou, C. S. Lee, H. Zhao and W. Zhang, *Adv. Mater.*, 2018, **30**, 1803144.
97. W. Cheng, H. Zhang, X. Zhao, H. Su, F. Tang, J. Tian and Q. Liu, *J. Mater. Chem. A*, 2018, **6**, 9420-9427.
98. H. Liang, A. N. Gandi, D. H. Anjum, X. Wang, U. Schwingenschlögl and H. N. Alshareef, *Nano Lett.*, 2016, **16**, 7718-7725.
99. Q. Liu, J. Huang, Y. Zhao, L. Cao, K. Li, N. Zhang, D. Yang, L. Feng and L. Feng, *Nanoscale*, 2019, DOI: 10.1039/C9NR00658C.
100. T. Chen, R. Zhang, G. Chen, J. Huang, W. Chen, X. Wang, D. Chen, C. Li and K. Ostrikov, *Catal. Today*, 2019, **337**, 147-154.
101. L. Hui, Y. Xue, B. Huang, H. Yu, C. Zhang, D. Zhang, D. Jia, Y. Zhao, Y. Li, H. Liu and Y. Li, *Nat. Commun.*, 2018, **9**, 5309.
102. X. Li, X. Hao, Z. Wang, A. Abudula and G. Guan, *J. Power Sources*, 2017, **347**, 193-200.
103. B. Weng, F. Xu, C. Wang, W. Meng, C. R. Grice and Y. Yan, *Energy Environ. Sci.*, 2017, **10**, 121-128.
104. R. Yang, Y. Zhou, Y. Xing, D. Li, D. Jiang, M. Chen, W. Shi and S. Yuan, *Appl. Catal., B*, 2019, **253**, 131-139.
105. Q. Q. Chen, C. C. Hou, C. J. Wang, X. Yang, R. Shi and Y. Chen, *Chem. Commun.*, 2018, **54**, 6400-6403.
106. C. Guan, W. Xiao, H. Wu, X. Liu, W. Zang, H. Zhang, J. Ding, Y. P. Feng, S. J. Pennycook and J. Wang, *Nano Energy*, 2018, **48**, 73-80.
107. Z. Li, W. Niu, L. Zhou and Y. Yang, *ACS Energy Letters*, 2018, **3**, 892-898.
108. H. Li, S. Chen, Y. Zhang, Q. Zhang, X. Jia, Q. Zhang, L. Gu, X. Sun, L. Song and X. Wang, *Nat. Commun.*, 2018, **9**, 2452.
109. C. Hu, L. Zhang, Z. J. Zhao, A. Li, X. Chang and J. Gong, *Adv. Mater.*, 2018, **30**, 1705538.
110. Z. Kang, H. Guo, J. Wu, X. Sun, Z. Zhang, Q. Liao, S. Zhang, H. Si, P. Wu, L. Wang and Y. Zhang, *Adv. Funct. Mater.*, 2019, **29**, 1807031.
111. J. Liu, Y. Zheng, Y. Jiao, Z. Wang, Z. Lu, A. Vasileff and S. Z. Qiao, *Small*, 2018, **14**, 1704073.
112. L. Zhou, M. Shao, J. Li, S. Jiang, M. Wei and X. Duan, *Nano Energy*, 2017, **41**, 583-590.
113. D. Senthil Raja, H. W. Lin and S. Y. Lu, *Nano Energy*, 2019, **57**, 1-13.
114. W. Ye, X. Fang, X. Chen and D. Yan, *Nanoscale*, 2018, **10**, 19484-19491.
115. Y. Wang, Y. Zhang, Z. Liu, C. Xie, S. Feng, D. Liu, M. Shao and S. Wang, *Angew. Chem. Int. Ed.*, 2017, **56**, 5867-5871.
116. Z. Cai, X. Bu, P. Wang, W. Su, R. Wei, J. C. Ho, J. Yang and X. Wang, *J. Mater. Chem. A*, 2019, DOI: 10.1039/C9TA07282A.
117. G. F. Chen, T. Y. Ma, Z. Q. Liu, N. Li, Y. Z. Su, K. Davey and S. Z. Qiao, *Adv. Funct. Mater.*, 2016, **26**, 3314-3323.
118. Z. Lu, W. Zhu, X. Yu, H. Zhang, Y. Li, X. Sun, X. Wang, H. Wang, J.

Wang, J. Luo, X. Lei and L. Jiang, *Adv. Mater.*, 2014, **26**, 2683-2687.
119. H. Sun, Z. Yan, F. Liu, W. Xu, F. Cheng and J. Chen, *Adv. Mater.*, 2019, **0**, 1806326.
120. Z. Yan, H. Sun, X. Chen, H. Liu, Y. Zhao, H. Li, W. Xie, F. Cheng and J. Chen, *Nat. Commun.*, 2018, **9**, 2373.
121. M. Asnavandi, Y. Yin, Y. Li, C. Sun and C. Zhao, *ACS Energy Letters*, 2018, **3**, 1515-1520.
122. Y. Wang, M. Qiao, Y. Li and S. Wang, *Small*, 2018, **14**, 1800136.
123. M. Q. Yang, J. Wang, H. Wu and G. W. Ho, *Small*, 2018, **14**, 1703323.
124. Y. Zhao, X. Zhang, X. Jia, G. I. N. Waterhouse, R. Shi, X. Zhang, F. Zhan, Y. Tao, L. Z. Wu, C. H. Tung, D. O'Hare and T. Zhang, *Adv. Energy Mater.*, 2018, **8**, 1703585.
125. J. Ping, Y. Wang, Q. Lu, B. Chen, J. Chen, Y. Huang, Q. Ma, C. Tan, J. Yang, X. Cao, Z. Wang, J. Wu, Y. Ying and H. Zhang, *Adv. Mater.*, 2016, **28**, 7640-7645.
126. H. Liu, Y. Wang, X. Lu, Y. Hu, G. Zhu, R. Chen, L. Ma, H. Zhu, Z. Tie, J. Liu and Z. Jin, *Nano Energy*, 2017, **35**, 350-357.
127. X. Long, S. Xiao, Z. Wang, X. Zheng and S. Yang, *Chem. Commun.*, 2015, **51**, 1120-1123.
128. A. L. Wang, H. Xu and G. R. Li, *ACS Energy Letters*, 2016, **1**, 445-453.
129. D. Friebel, M. W. Louie, M. Bajdich, K. E. Sanwald, Y. Cai, A. M. Wise, M. J. Cheng, D. Sokaras, T. C. Weng and R. Alonso-Mori, *J. Am. Chem. Soc.*, 2015, **137**, 1305-1313.
130. M. Gong, W. Zhou, M. J. Kenney, R. Kapusta, S. Cowley, Y. Wu, B. Lu, M. C. Lin, D. Y. Wang, J. Yang, B. J. Hwang and H. Dai, *Angew. Chem. Int. Ed.*, 2015, **54**, 11989-11993.
131. X. Li, L. Zhang, M. Huang, S. Wang, X. Li and H. Zhu, *J. Mater. Chem. A*, 2016, **4**, 14789-14795.
132. J. Luo, D. A. Vermaas, D. Bi, A. Hagfeldt, W. A. Smith and M. Grätzel, *Adv. Energy Mater.*, 2016, **6**, 1600100.
133. C. G. Morales-Guio, M. T. Mayer, A. Yella, S. D. Tilley, M. Grätzel and X. Hu, *J. Am. Chem. Soc.*, 2015, **137**, 9927-9936.
134. W. He, R. Wang, L. Zhang, J. Zhu, X. Xiang and F. Li, *J. Mater. Chem. A*, 2015, **3**, 17977-17982.
135. M. Arif, G. Yasin, M. Shakeel, X. Fang, R. Gao, S. Ji and D. Yan, *Chem. Asian J.*, 2018, **13**, 1045-1052.
136. M. Arif, G. Yasin, M. Shakeel, M. A. Mushtaq, W. Ye, X. Fang, S. Ji and D. Yan, *Mater. Chem. Front.*, 2019, **3**, 520-531.

